

Sufficient principal component regression for pattern discovery in transcriptomic data

Lei Ding
Department of Statistics
Indiana University
Bloomington, IN USA

Gabriel E. Zentner
Department of Biology
Melvin and Bren Simon Comprehensive Cancer Center
Indiana University
Bloomington, IN USA

Daniel J. McDonald
Department of Statistics
University of British Columbia
Vancouver, BC Canada

July 6, 2021

Abstract

Methods for global measurement of transcript abundance such as microarrays and RNA-seq generate datasets in which the number of measured features far exceeds the number of observations. Extracting biologically meaningful and experimentally tractable insights from such data therefore requires high-dimensional prediction. Existing sparse linear approaches to this challenge have been stunningly successful, but some important issues remain. These methods can fail to select the correct features, predict poorly relative to non-sparse alternatives, or ignore any unknown grouping structures for the features. We propose a method called SuffPCR that yields improved predictions in high-dimensional tasks including regression and classification, especially in the typical context of omics with correlated features. SuffPCR first estimates sparse principal components and then estimates a linear model on the recovered subspace. Because the estimated subspace is sparse in the features, the resulting predictions will depend on only a small subset of genes. SuffPCR works well on a variety of simulated and experimental transcriptomic data, performing nearly optimally when the model assumptions are satisfied. We also demonstrate near-optimal theoretical guarantees.

1 Introduction

Global transcriptome measurement with microarrays and RNA-seq is a staple approach in many areas of biological research and has yielded numerous insights into gene regulation. Given data from such experiments, it is often desirable to identify a small number of transcripts whose expression levels are associated with a phenotype of interest (for instance, disease-free survival of cancer patients). Indeed, projects such as The Cancer Genome Atlas (TCGA) have aimed to generate massive volumes of such data to enable molecular characterization of various cancers. While these data are readily available, their high-dimensional nature (tens of thousands of transcript measurements from a single experiment) makes identification of a compact gene expression signature statistically and computationally challenging. While the identification of a minimal gene expression signature is valuable in evaluating disease prognosis, it is also helpful for guiding experimental exploration. In practical terms, a set of five genes highly associated with a certain disease phenotype

can be characterized more rapidly, at lower cost, and in more depth than a set of 50 or 100 such genes using genetic techniques such as CRISPR knockout and cancer biological methods such as xenotransplantation of genetically-modified cells into mice. Therefore, this paper prioritizes the ability to select a small subset of transcript measurements which nonetheless provide accurate prediction of phenotypes.

With these goals in mind, supervised linear regression techniques such as ridge regression [26], the lasso [46], elastic net [56], adaptive lasso [55], or other penalized methods are often employed. More commonly, especially in genomics applications, the outcomes of interest tend to be the result of groups of genes, which perhaps together describe more complicated processes. Therefore, researchers often turn to unsupervised methods such as principal component analysis (PCA), principal component regression (PCR), and partial least squares (PLS) for both preprocessing and as predictive models [2, 9, 14, 21, 30, 31, 36, 47, 51, 53].

1.1 Recent related work

PCA has two main drawbacks when used in high dimensions. The first is that PCA is non-sparse, so it uses information from all the available genes instead of selecting only those which are important, a key objective in omics applications. That is, the right singular vectors or “eigengenes” [1] depend on all the genes measured rather than a small collection. The second is that these sample principal components are not consistent estimators of the population parameters in high dimensions [29]. This means essentially that when the number of patients is smaller than the number of genes, even if the first eigengene could perfectly explain the data, PCA will not be able to recover it.

Modern approaches developed specifically for the genomics context such as supervised gene shaving [23], tree harvesting [24], and supervised principal components (SPC) [5, 6, 42] have sought to combine the presence of the phenotype with the structure estimation properties of eigendecompositions on the gene expression measurements using unsupervised techniques to obtain the best of both. PLS has long been common in genomics [10, 11, 33], though it remains uncommon in statistics and machine learning, and its theoretical properties are poorly understood. Other recent PCA-based approaches for genetics, though not directly applicable for prediction are SMSSVD [25] and ESPCA [39].

1.2 Contributions

In this paper, we attempt to leverage the strong theoretical properties associated with sparse PCA techniques to improve predictive accuracy with sparsity for regression and classification problems in genomics. We are able to avoid the strong assumptions necessary for SPC, the current state-of-the-art, while obtaining the benefits associated with sparse subspace estimation. In the case that the phenotype is actually generated as a linear function of a handful of genes, our method, SuffPCR, performs nearly optimally: it does as well as if we had known which genes were relevant beforehand. Furthermore, we justify theoretically that our procedure can both predict accurately and recover the correct genes. Our contributions can be succinctly summarized as follows:

1. We present a methodology for discovering small sets of predictive genes using sparse PCA;
2. Our method improves the computational properties of existing sparse subspace estimation approaches to enable previously impossible inference when the number of genes is very large;
3. We demonstrate state-of-the-art performance of our method in synthetic examples and with standard cancer microarray measurements;

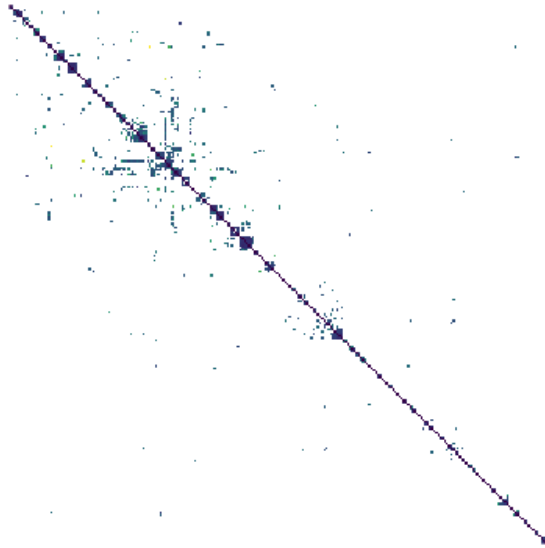


Figure 1: An estimate of the precision matrix for the first 250 genes from the AML dataset with 99% of the off-diagonal elements equal to 0. Darker colors represent larger magnitude correlations.

4. We provide near-optimal theoretical guarantees.

In [Section 2](#), we motivate the desire for *sufficient* PCR relative to previous approaches and present details of SuffPCR. [Section 3](#) illustrates performance in simulated, semi-simulated, and real examples and discusses the biological implications of our methods for a selection of cancers. [Section 4](#) gives theoretical justifications for our methods, providing guarantees for prediction accuracy and correct gene selection. [Section 5](#) concludes.

Notation. We use bold uppercase letters to denote matrices, lowercase Arabic letters to denote row vectors and scalars, and uppercase Arabic letters for column vectors. Let Y be a real-valued n -vector of a phenotype, and \mathbf{X} be the rowwise concatenation of i.i.d. draws x_i from a distribution on \mathbb{R}^p with covariance Σ (a set of transcriptomic measurements for a patient). We will assume throughout, without loss of generality, that $\mathbb{E}[x_i] = 0$, and that \mathbf{X} has been centered. The singular value decomposition (SVD) of a matrix \mathbf{A} is $\mathbf{A} = \mathbf{U}(\mathbf{A})\Lambda(\mathbf{A})\mathbf{V}^\top(\mathbf{A})$. In the specific case of \mathbf{X} , we suppress the dependence on \mathbf{X} in the notation and write $\mathbf{X} = \mathbf{U}\Lambda\mathbf{V}^\top$. We write \mathbf{A}_d to indicate the first d columns of the matrix \mathbf{A} and a_j to denote the j^{th} row. In the case of the identity matrix, we use a subscript to denote its dimension when necessary: \mathbf{I}_p . Let $\text{tr}(\mathbf{A})$ denote the sum of the diagonal entries of \mathbf{A} while $\|\mathbf{A}\|_F^2 = \sum_{ij} a_{ij}^2$ is the squared Frobenius norm of \mathbf{A} . $\|\mathbf{A}\|_{2,0}$ denotes $(2,0)$ -norm of \mathbf{A} , that is the number of rows in \mathbf{A} that have non-zero ℓ_2 norm. $\|\mathbf{A}\|_{1,1}$ is the sum of the row-wise ℓ_1 -norms.

2 Motivation and methodology

Supervised Principal Components [[5](#), [6](#), [42](#)] is widely used for solving high-dimensional prediction and feature selection problems. It targets dimension reduction and sparsity simultaneously by first screening genes (or individual mRNA probes) based on their marginal correlation with the

% sparsity of Σ^{-1}	100	99.9	99.6	98.9	97.5	95.3
% non-zero β^* 's	1.8	3.3	8.4	23.5	50.2	77.9
False negative rate	0.000	0.431	0.778	0.921	0.963	0.976

Table 1: Illustration of the failure of Equation (1) on the AML data.

phenotype (or likelihood ratio test in the case of non-Gaussian noise). Then, it performs PCA on this selected subset and regresses the phenotype on the resulting components (possibly with additional penalization). This procedure is computationally simple, but, zero population marginal correlation is neither necessary nor sufficient to guarantee that the associated population regression coefficient is zero. To make this statement mathematically precise, consider the linear model $y = x^\top \beta^* + \epsilon$, where y is a real-valued scalar phenotype, x is real-valued vector of genes, β^* is the true (unknown) coefficient vector, and ϵ is a mean-zero error. Defining $\text{Cov}(x, x) = \Sigma$, and $\text{Cov}(x, y) = \Phi$, this procedure requires that

$$\Phi_j = 0 \Rightarrow \beta_j^* = (\Sigma^{-1}\Phi)_j = 0. \quad (1)$$

In words, we are assuming that the dot product of the j^{th} row of the precision matrix with the marginal covariance between x and y is zero whenever the j^{th} element of Φ is zero. To illustrate why this assumption fails for genomics problems, we examine a motivating counterexample. Using mRNA measurements for acute myeloid leukemia (AML, the same data examined below, Bullinger et al. 8), we estimate both Σ^{-1} and Φ and proceed as if these estimates are the population quantities. To estimate Φ , we use the empirical covariance and set all but the largest $n = 116$ values equal to zero, corresponding to a sparse solution. For Σ^{-1} , we use the Graphical Lasso [17] for all $p = 6283$ genes at different sparsity levels ranging from 100% sparse ($\hat{\Sigma}_{ij} = 0$ for all $i \neq j$) to 95% sparse. We then create $\beta^* = \Sigma^{-1}\Phi$ as in Equation 1. This is essentially the most favorable condition for SPC. For visualization purposes, Figure 1 shows the estimated precision matrix of the first 250 genes at 99% sparsity.

Table 1 shows the sparsity of the precision matrix, the percentage of non-zero regression coefficients, and the percentage of non-zero regression coefficients which are incorrectly ignored under the assumption (the false negative rate). Even if the precision matrix is 99.9% sparse, the false negative rate is over 40%, meaning that we find fewer than 60% of the true genes. If the sparsity of Σ^{-1} is allowed to decrease only slightly, the false negative rate increases to over 95%. Clearly, this screening procedure is likely to ignore many important genes in even the most favorable conditions for SPC.

More recent work has attempted to avoid this assumption. Ding and McDonald [15] uses the initially selected set of features to approximate the information lost in the screening step via techniques from numerical linear algebra. An alternative approach discussed in Piironen and Vehtari [43] iterates the screening step with the prediction step, adding back features which correlate with the residual. Finally, Tay et al. [45] tackles the computational complexity directly when the grouping structure is known and estimates separate subspaces for different groups of features. All these methodologies are tailored to perform well when Φ and β^* have particular compatible structures.

On the other hand, it is important to observe that a sufficient condition for $\beta_j^* = 0$ in Equation (1) is that the j^{th} row of the left eigenvectors of Σ is 0. Based on this intuition, we develop sufficient PCR (abbreviated as SuffPCR) which leverages this insight: row sparse eigenvectors imply sparse coefficients, and hence depend on only a subset of genes. SuffPCR is tailored to the case that \mathbf{X} lies approximately on a low-dimensional linear manifold which depends on a small subset of features. Because the linear manifold depends on only some of the features, β^* does as well.

2.1 Prediction with principal components

PCA is a canonical unsupervised dimension reduction method when it is reasonable to imagine that \mathbf{X} lies on (or near) a low-dimensional linear manifold. It finds the best d -dimensional approximation of the span of \mathbf{X} such that the reconstruction error in ℓ_2 norm is minimized. This problem is equivalent to maximizing the variance explained by the projection:

$$\max_{\mathbf{V}} \operatorname{tr}(\mathbf{S}\mathbf{V}\mathbf{V}^\top) \quad \text{subject to} \quad \mathbf{V}^\top \mathbf{V} = \mathbf{I}_d, \quad (2)$$

where $\mathbf{S} = \frac{1}{n} \mathbf{X}^\top \mathbf{X}$ is the sample covariance matrix. Let $\mathbf{X} = \mathbf{U}\mathbf{\Lambda}\mathbf{V}^\top$, then the solution of this optimization problem is \mathbf{V}_d , the first d right singular vectors, and the estimator of the first d principal components is $\mathbf{U}_d\mathbf{\Lambda}_d$ or $\mathbf{X}\mathbf{V}_d$ equivalently. Given an estimate of the principal components, principal component regression (PCR) is simply ordinary least squares (OLS) regression of the phenotype on the derived components $\mathbf{U}_d\mathbf{\Lambda}_d$. One can convert the lower-dimensional estimator, say $\hat{\gamma}$, back to the original space to reacquire an estimator of β^* as $\hat{\beta} = \mathbf{V}_d\hat{\gamma}$. Other generalized linear models can be used place of OLS to find $\hat{\gamma}$.

2.2 Sparse principal component analysis

As discussed in [Section 1.1](#), standard PCA works poorly in high dimensions. Much like the high-dimensional regression problem, estimating high-dimensional principal components is ill-posed without additional structure. To address this issue many authors have focused on different sparse PCA estimators for the case when \mathbf{V} is sparse in some sense. Many of these methods achieve this goal by adding a penalty to Equation (2). Of particular utility for the case of PCR when β^* is sparse is to choose a penalty that results in row-sparse \mathbf{V} . This intuition is justified by the following result.

Proposition 1. *Consider the linear model $y = x^\top \beta^* + \epsilon$ with $\operatorname{Cov}(x, x) = \mathbf{\Sigma}$. Let $\mathbf{\Sigma} = \mathbf{V}(\mathbf{\Sigma})\mathbf{\Lambda}(\mathbf{\Sigma})\mathbf{V}(\mathbf{\Sigma})^\top$ be the eigendecomposition of $\mathbf{\Sigma}$ with $\mathbf{\Lambda}(\mathbf{\Sigma})_{jj} = 0$ for $j > d \in \mathbb{Z}^+$. Then $\|v(\mathbf{\Sigma})_j\|_2 = 0 \Rightarrow \beta_j^* = 0$.*

The proof is immediate. For any j , if $\|v(\mathbf{\Sigma})_j\|_2 = 0$, then every element in $v(\mathbf{\Sigma})_j$ is 0, indicating the j^{th} row of $\mathbf{\Sigma}^{-1}$ will be 0. Since $\beta_j^* = (\mathbf{\Sigma}^{-1}\Phi)_j$ where $\operatorname{Cov}(x, y) = \Phi$, it also results in $\beta_j^* = 0$.

This result stands in stark contrast to the assumption in Equation (1). This proposition gives a guarantee rather than requiring an assumption: if the rows of \mathbf{V}_d are sparse, then β_* is sparse. The same intuition can easily be extended to the case $\mathbf{\Lambda}(\mathbf{\Sigma})_{jj} \geq 0$ for all j given a gap between the d^{th} and $(d+1)^{\text{st}}$ eigenvalues.

In this setting, the natural analogue of PCA is the solution to the following penalized version:

$$\max_{\mathbf{V}} \langle \mathbf{S}, \mathbf{V}\mathbf{V}^\top \rangle - \lambda \|\mathbf{V}\|_{2,0}^2 \quad \text{subject to} \quad \mathbf{V}^\top \mathbf{V} = \mathbf{I}_d. \quad (3)$$

Solutions $\hat{\mathbf{V}}_d$ of Equation (3) will give projection matrices onto the best d -dimensional linear manifold such that $\hat{\mathbf{V}}_d$ is row sparse. However, this problem is NP-hard.

Many authors have developed different versions of sparse PCA. For example, d'Aspremont et al. [12] and Zou et al. [57] focus on the first principal component and add additional principal components iteratively to account for the variation left unexplained by the previous principal components. However, such approaches result in non-orthogonal components. Vu and Lei [49] derives a rate-minimax lower bound, illustrating that no estimator can approach the population quantity faster than, essentially, $q\sqrt{d/n}$ where q is a deterministic function of $\mathbf{\Sigma}$. Later work in Vu

et al. [50] proposes a convex relaxation to Equation (3) which finds the first d principal components simultaneously and nearly achieves the lower bound:

$$\max_{\mathbf{V}} \operatorname{tr}(\mathbf{S}\mathbf{V}\mathbf{V}^\top) - \lambda \|\mathbf{V}\mathbf{V}^\top\|_{1,1} \quad \text{subject to } \mathbf{V}\mathbf{V}^\top \in \mathcal{F}^d, \quad (4)$$

where $\mathcal{F}^d := \{\mathbf{V}\mathbf{V}^\top : \mathbf{0} \preceq \mathbf{V}\mathbf{V}^\top \preceq \mathbf{I}_p \text{ and } \operatorname{tr}(\mathbf{V}\mathbf{V}^\top) = d\}$ is a convex body called Fantope, motivating the name Fantope Projection and Selection (FPS). The authors solve the optimization problem in Equation (4) with an alternating direction method of multipliers (ADMM) algorithm.

For these reasons, FPS is known as the current state-of-the-art sparse PCA estimator with the best performance. However, despite its theoretical justification, FPS is less useful in practice for solving prediction tasks, especially in genomics applications with $p \gg n$ (rather than just $p > n$) for two reasons. First, the original ADMM algorithm has per-iteration computational complexity $\mathcal{O}(p^3)$, which is a burden especially when p is large. Secondly, because of the convex relaxation using Equation 4 rather than Equation 3, $\widehat{\mathbf{V}}_d$ from FPS tends to be entry-wise sparse, but infrequently row-wise sparse unless the signal-to-noise ratio (SNR) is very large (q is a function of this ratio). In genomics applications with low SNR, which is common, estimates $\widehat{\beta}$ tend to have large numbers of non-zero coefficients with very small estimated values. Thus we design SuffPCR based on the insights from Proposition 1, utilizing the best sparse PCA estimator FPS, and further addressing both of these issues to achieve better empirical performance while maintaining theoretical justification.

2.3 Sufficient principal component regression

In this section, we introduce a new method for high-dimensional prediction called SuffPCR. The main idea of SuffPCR is to detect the relationship between the phenotype Y and gene expression measurements \mathbf{X} by making use of the (near) low-dimensional manifold that supports \mathbf{X} . In broad outline, SuffPCR first uses a tailored version of FPS to produce a row-sparse estimate $\widehat{\mathbf{V}}_d$, and then regresses Y on the derived components to produce sparse coefficient estimates. SuffPCR for regression is stated in Algorithm 1 and summarized visually in Figure 2. For ease of exposition, we remind the reader that Y and \mathbf{X} are standardized so that $\mathbf{S} = \frac{1}{n}\mathbf{X}^\top\mathbf{X}$ is the correlation matrix.

The first issue is the time complexity of the original FPS algorithm. Essentially, FPS uses the same three steps depicted in lines 4, 5, and 6 in Algorithm 1:

- 4'. $\mathbf{A} \leftarrow \operatorname{Proj}_{\mathcal{F}^d}(\mathbf{B} - \mathbf{C} + \mathbf{S}/\rho)$
5. $\mathbf{B} \leftarrow \operatorname{Soft}_{\lambda/\rho}(\mathbf{A} + \mathbf{C})$ where $\operatorname{Soft}_a(b) = \operatorname{sign}(b)(|b| - a)_+$
6. $\mathbf{C} \leftarrow \mathbf{C} + \mathbf{A} - \mathbf{B}$.

The only difference here between our implementation and that in FPS is in step 4 (resp. 4'). Each step takes a matrix and produces another matrix, where the matrices have p^2 elements. The second step is element-wise soft-thresholding while the third is simply matrix addition, so both are simple to calculate. But the first, $\operatorname{Proj}_{\mathcal{F}^d}(\mathbf{Q})$, requires two operations. The first is the eigendecomposition of \mathbf{Q} , an $\mathcal{O}(p^3)$ operation. The second modifies the eigenvalues of \mathbf{Q} through the solution of a piecewise linear equation in τ : $\Lambda_{i,+}^2(\mathbf{Q}) = \min\{\max\{\Lambda_i^2(\mathbf{Q}) - \tau, 0\}, 1\}$, with τ such that $\sum_{i=1}^{n \wedge p} \Lambda_{i,+}^2(\mathbf{Q}) = d$. The final result is then reconstructed as $\mathbf{A} = \mathbf{U}(\mathbf{Q})\Lambda_+^2(\mathbf{Q})\mathbf{U}(\mathbf{Q})^\top$. Because of the cubic complexity in p , the authors suggest the number of features should not exceed one thousand. But typical transcriptomics data has many thousands of gene measurements, and preliminary selection of a subset is suboptimal, as illustrated above.

Due to the form of the piecewise solution, most eigenvalues will be set to 0. Thus, while we will generally require more than d eigenpairs, most are unnecessary, certainly fewer than $\min\{n, p\}$. Therefore, SuffPCR solves the eigendecomposition approximately, replacing $\operatorname{Proj}_{\mathcal{F}^d}$ with $\widetilde{\operatorname{Proj}}_{\mathcal{F}^d}$. Our implementation computes only a handful of eigenvectors corresponding to the largest eigenvalues,

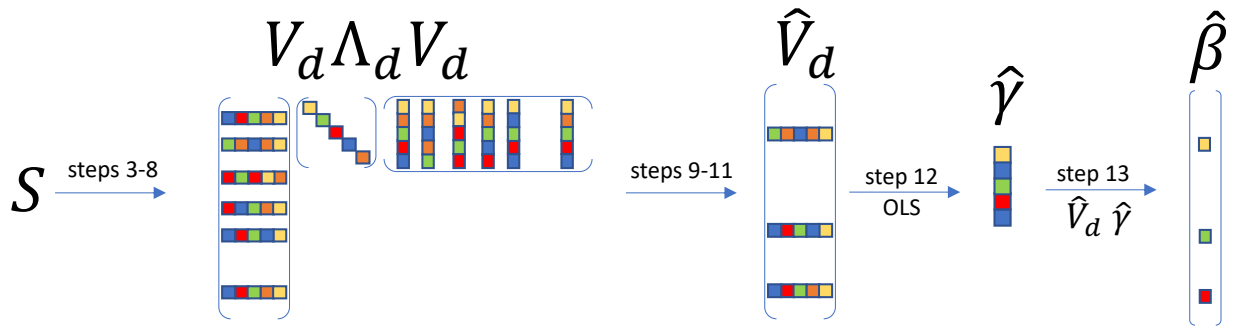


Figure 2: Graphical depiction of [Algorithm 1](#). Solid colors represent matrix entries while empty space represents 0.

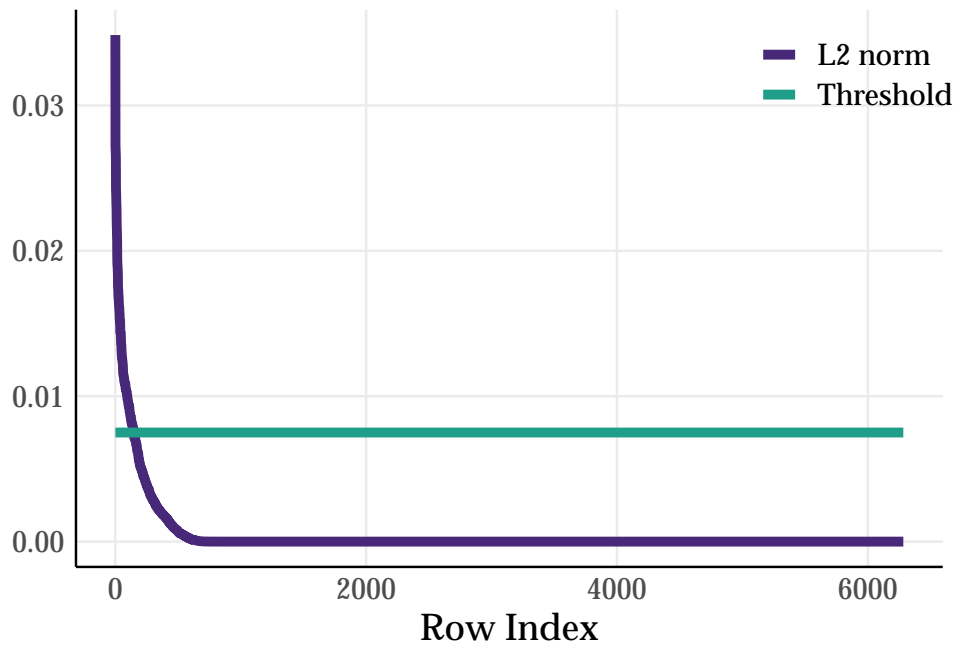


Figure 3: This figure shows the curve of the sorted ℓ_2 norm of rows in \hat{V}_d in one iteration of SuffPCR on the AML dataset. The threshold t is selected by [Algorithm 2](#).

Algorithm 1 SuffPCR (regression version)

- 1: **Input:** $\mathbf{X}, \mathbf{S}, Y, d, \lambda, \rho$
- 2: $\mathbf{B} \leftarrow \mathbf{0}, \mathbf{C} \leftarrow \mathbf{0}$
- 3: **while** not converged **do**
- 4: $\mathbf{A} \leftarrow \widetilde{\text{Proj}}_{\mathcal{F}^d}(\mathbf{B} - \mathbf{C} + \mathbf{S}/\rho)$
- 5: $\mathbf{B} \leftarrow \text{Soft}_{\lambda/\rho}(\mathbf{A} + \mathbf{C})$
- 6: $\mathbf{C} \leftarrow \mathbf{C} + \mathbf{A} - \mathbf{B}$
- 7: **end while**
- 8: Decompose $\mathbf{B} = \mathbf{V}_d \mathbf{\Lambda}_d \mathbf{V}_d^\top$
- 9: Compute $l = \mathbf{diag}(\mathbf{V}_d \mathbf{V}_d^\top)$, sort in descending order
- 10: Apply [Algorithm 2](#) to l and get t
- 11: Set rows in \mathbf{V}_d whose ℓ_2 norm is smaller than t as 0, and get $\widehat{\mathbf{V}}_d$
- 12: Solve $\widehat{\gamma} = \text{argmin}_{\gamma} \left\| Y - \mathbf{X} \widehat{\mathbf{V}}_d \gamma \right\|_2^2$
- 13: **Return:** $\widehat{\beta} = \widehat{\mathbf{V}}_d \widehat{\gamma}$

Algorithm 2 find threshold t

- 1: **Input:** a p -vector l
- 2: **for** $i \in 1, \dots, p$ **do**
- 3: $T_n[i] = \text{var}(l[1 : i])$
- 4: $T_s[i] = \text{var}(l[(i + 1) : p])$
- 5: $T[i] = i * T_n[i] + (p - i) T_s[i]$
- 6: $\delta[i] = T[i] - T[i - 1]$ \triangleright empirical derivative of T
- 7: **end for**
- 8: Set $i^* = \text{argmin}_i \{ \delta[i] - \delta[i - 1] > \text{mean}(|\delta[1 : (i - 1)]|) \}$
- 9: **Return:** $t = l[i^*]$

rather than all p . If we compute enough to ensure that some $\mathbf{\Lambda}_{i,+}^2(\mathbf{Q})$ will be 0, then the rest are as well. Our implementation uses Augmented Implicitly Restarted Lanczos Bidiagonalization [AIRLB, 3] as implemented in the `irlba` package [4], though alternative techniques such as those in Gittens and Mahoney [18], Halko et al. [20], Homrighausen and McDonald [27] may work as well. We provide a more detailed discussion of this approximate implementation in the Supplement.

For moderate problems ($n = 100$ and $p = 500$), computing the truncated eigendecomposition using AIRLB rather than the full eigendecomposition leads to a three-fold speedup while the further incorporation of specialized initializations leads to an eight-fold improvement without any discernable loss of accuracy (results on a 2018 MacBook Pro with 2.7 GHz Quad-Core processor and 16GB of memory running macOS 10.15). The results are similar when $p = 5000$, though the same experiment on a high-performance Intel Xeon E5-2680 v3 CPU with 12 cores, 256GB of memory, and optimized BLAS were somewhat less dramatic (improvements of three-fold and four-fold respectively). For large RNA-Seq datasets ($p \approx 20000$), we observed a nearly ten-fold improvement in computation time.

The second issue of FPS is that the Fantope constraint in Equation (4) ensures only that $\text{tr}(\mathbf{V}\mathbf{V}^\top) = d$ but not that the number of rows with non-zero ℓ_2 -norm is small. This feature of the convex relaxation frequently results in many rows with very small, but non-zero, row-norm resulting in dense estimates of β^* . Thus, to make the final estimator $\widehat{\mathbf{V}}_d$ sparse, we hard-threshold rows in $\widehat{\mathbf{V}}_d$ whose ℓ_2 norm is small, as illustrated in line 9, 10, and 11 in [Algorithm 1](#). From empirical experience, we have found that there is often a strong elbow-type behavior in the row-wise ℓ_2 norm of $\widehat{\mathbf{V}}_d$,

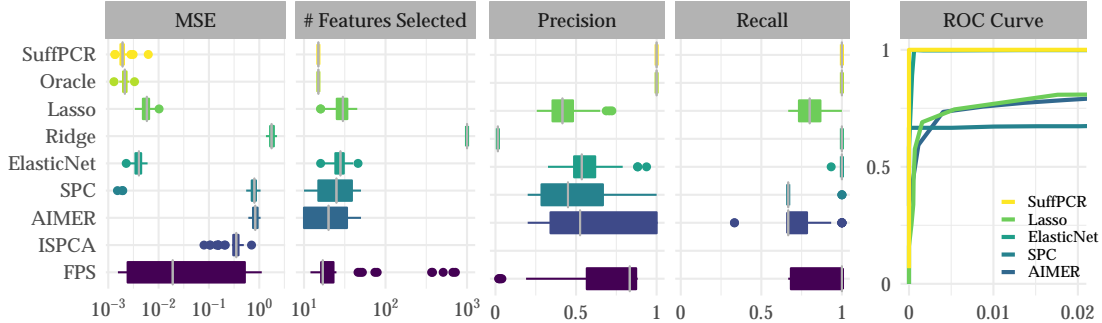


Figure 4: This figure compares the performance of SuffPCR against alternatives when the features come from a row-sparse factor model under favorable conditions for SuffPCR. Boxplots and ROC curve are over 50 replications. The x -axis is on the log scale in the left two plots. We have omitted the other methods from the ROC curve for legibility, but their behavior is similar to lasso.

similar to the Skree plot used to choose d in standard PCA as shown in Figure 3. Therefore, we develop Algorithm 2 to find the best threshold automatically by calculating the empirical derivative of the observation-weighted variances on each side of a potential threshold. With this algorithm, we produce a threshold that maximizes the difference between the variances of the “signal” and “noise” rows. We then set the rows in $\hat{\mathbf{V}}_d$ corresponding to the noise to 0. SuffPCR is also amenable for solving other generalized linear model problems. For example, to solve classification problems, one simply uses logistic regression in line 12 of Algorithm 1.

3 Empirical evaluations

In this section, we show how SuffPCR performs on synthetic data and on real public genomics datasets relative to state-of-the-art methods. Section 3.1 first presents a generative model for synthetic data and motivates the assumptions required for our theoretical results in Section 4. As our procedure is intended to improve upon SPC, we include two main simulation settings: (1) conditions favorable to SuffPCR relative to SPC; and (2) scenarios favorable to SPC. We also investigate the influence of tuning parameter selection and signal to noise ratio (see the Supplement). Section 3.2 uses the NSCLC data as the \mathbf{X} matrix, but creates the response from a linear model. Section 3.3 reports the performance of SuffPCR on 5 public genomics datasets. The supplement includes similar results for binary survival-status outcomes. Across most settings in both synthetic and real data, SuffPCR outperforms all competitors in prediction mean-squared error and is able to select the true genes (those with $\beta^* \neq 0$) more accurately.

3.1 Synthetic data experiments

We generate data from the multivariate Gaussian linear model $y_i = x_i^\top \beta^* + \sigma_y \epsilon_i$, where $x_i \sim N_p(0, \Sigma)$, β^* is the p -dimensional regression coefficient, $\epsilon_i \sim N(0, 1)$, and $\sigma_y > 0$. We impose an orthogonal factor model for the covariates $\mathbf{X} = \mathbf{U}_d \mathbf{\Lambda}_d \mathbf{V}_d^\top + \sigma_x \mathbf{E}$, where the rows of \mathbf{U}_d follow $N_d(0, \mathbf{I}_d)$ independently, $\mathbf{\Lambda}_d$ is a diagonal matrix with entries $(\lambda_1, \dots, \lambda_d)$ in descending order, and $\mathbf{V}_d \in \mathbb{R}^{p \times d}$ with $\mathbf{V}_d^\top \mathbf{V}_d = \mathbf{I}_d$. The noise \mathbf{E} is an $n \times p$ matrix with i.i.d. $N(0, 1)$ entries independent of \mathbf{U}_d , and $\lambda_d > \sigma_x > 0$. We assume \mathbf{V}_d is row sparse with only s rows containing non-zero entries. These non-zero rows are the “true” features to be discovered, and they correspond to $\beta^* \neq 0$. Under this

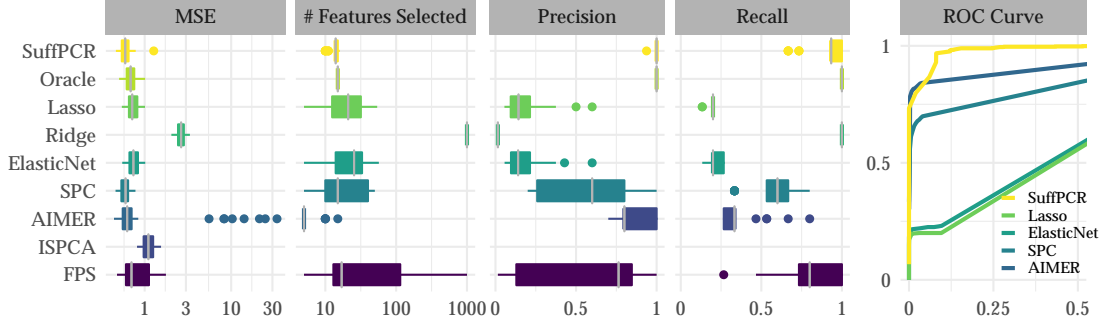


Figure 5: This figure demonstrates the performance of SuffPCR under favorable conditions for SPC. We have omitted the other methods from the ROC curve for legibility, but their behavior is similar to lasso.

model, the rows of \mathbf{X} follow a multivariate Gaussian distribution independently, with mean 0 and covariance $\Sigma = \mathbf{V}\mathbf{L}\mathbf{V}^\top$, where the eigenvalues $l_1 \geq \dots \geq l_p \geq 0$ with $l_i = \lambda_i^2 I(i \leq d) + \sigma_x^2$.

We generate Y as a linear function of the latent factors \mathbf{U}_d with additive Gaussian noise: $Y = \mathbf{U}_d\Theta + \sigma_y Z$, where Θ is the regression coefficient, $\sigma_y > 0$ is a constant, and $Z \sim N_n(0, \mathbf{I})$, independent of \mathbf{X} . Under this model for \mathbf{X} and Y , the population marginal correlation between each feature in \mathbf{X} and Y is $\Phi = \mathbf{V}_d\mathbf{\Lambda}_d\Theta$, and the population ordinary least squares coefficient of regressing Y on \mathbf{X} is $\beta^* = \mathbf{V}_d\mathbf{L}_d^{-1}\mathbf{\Lambda}_d\Theta$. We define set $\mathcal{A} := \{j : \beta_j^* \neq 0\}$ and set $\mathcal{B} := \{j : \Phi_j \neq 0\}$. Note that the size of set \mathcal{A} is s , i.e. $|\{j : \beta_j^* \neq 0\}| = s$, because \mathbf{V}_d has only s rows with non-zero entries.

In all cases, we use $n = 100$ observations and $p = 1000$ features, generating three equal-sized sets for training, validation, and testing. We use prediction accuracy of the validation set to select any tuning parameters and the test set for evaluating out-of-sample performance. Each simulation is repeated 50 times. Results with $n = 200$ and $p = 5000$ were similar.

We compare SuffPCR with a number of alternative methods. The Oracle estimator uses ordinary least squares (OLS) on the true features and serves as a natural baseline: it uses information unavailable to the analyst (the true genes) but represents the best method were that information available. We also present results for Lasso [46], Ridge [26], Elastic Net [56], SPC [6], AIMER [15], ISPCA [43], and PCR using FPS directly without feature screening (using Algorithm 1 without step 9, 10 and 11). For ISPCA, we use the `dimreduce` R package to estimate the principal components before performing regression. Additional experiments are given in the Supplement.

3.1.1 Conditions favorable to SuffPCR

The first setting is designed to show the advantages of SuffPCR relative to alternative methods, especially SPC. We note that other methods that employ screening by the marginal correlation [15, 43] will have similar deficiencies. Because SPC works well if Equation (1) holds, we design Σ to violate this condition. We set the first 15 features to have non-zero β^* , but only the first 10 features have non-zero marginal correlation with the phenotype. We set the true dimension of the subspace as $d = 3$, and we use the correct dimension for methods based on principal components.

Figure 4 shows the performance of SuffPCR and state-of-the-art alternatives. In addition to reporting each method's prediction MSE on the test set, we also show the number of features selected, precision, recall as well as the ROC curve. The number of selected features for ISPCA is unavailable from the `dimreduce` package. In this example, SuffPCR actually outperforms the oracle

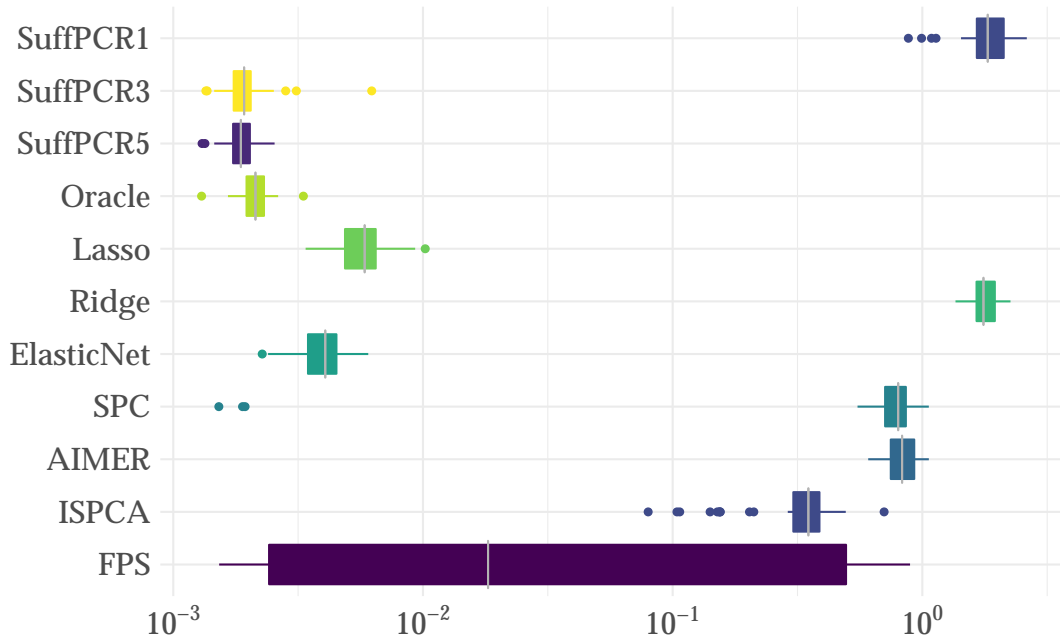


Figure 6: This figure compares the prediction MSE of SuffPCR with alternatives with different d in SuffPCR.

estimator, attaining smaller MSE while generally selecting the correct features. This seemingly implausible result is likely because the variance of estimating OLS on 15 features is large relative to that of estimating the low-dimensional manifold followed by 3 regression coefficients. SuffPCR has a clear advantage over all the alternative methods, especially SPC which is 3 orders of magnitude worse. SPC works so poorly because it ignores 5 features. ISPCA has slightly lower MSE than SPC. Ridge is the worst, due to fitting a dense model when a sparse model generated the data. SuffPCR reduces MSE significantly relative to simply using FPS due to more accurate feature selection. The right plot in Figure 4 further shows the ROC curve for SuffPCR, Lasso, Elastic Net, SPC and AIMER in which we can easily vary the tuning parameter and select various numbers of features. SuffPCR and AIMER have a perfect ROC curve, while the other 3 methods are unable to identify 5 features.

3.1.2 Conditions favorable to SPC

This example is designed to show the performance of SuffPCR under favorable conditions for SPC. Here, the only alteration to the data generation process is that we set the first 10 features to have non-zero β^* , the same features which have non-zero marginal correlations with the phenotype. Figure 5 gives the analogous results for this example. Here, SuffPCR has comparable MSE to SPC, which is the best, slightly better than the oracle as was the case for SuffPCR above. However, SPC is less likely to select the correct features, while SuffPCR selects the correct features most of the time. Furthermore, SuffPCR tends to select fewer features, and it has the best precision and recall (Ridge will always have recall equal to 1).

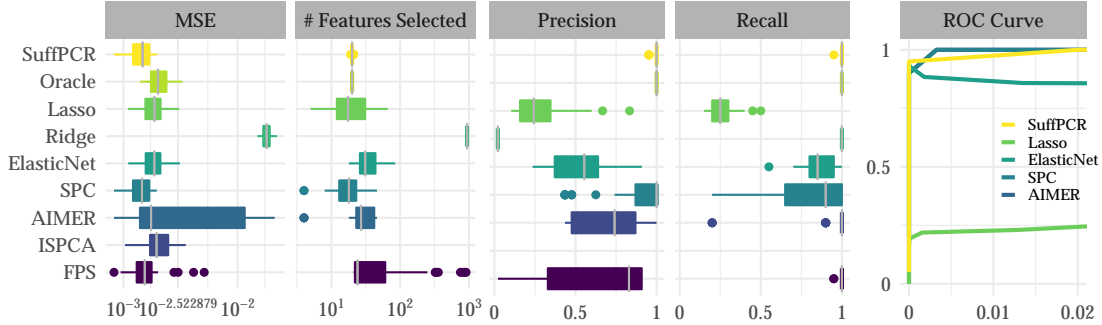


Figure 7: This figure compares the performance of SuffPCR against alternatives when the features come from a row-sparse factor model extracted from the NSCLC data. Boxplots and ROC curve are over 50 replications. The x -axis is on the log scale in the left two plots.

3.1.3 Selecting tuning parameters

In SuffPCR, the tuning parameters are the penalty term λ , the dimension of the projected subspace d , and the threshold t . In all the simulations, we examine the same values of λ . When analyzing real datasets, our algorithm offers automatic calculation of potential values of λ given the sample covariance matrix. In practice, the more penalty parameters we explore, the better the results could be assuming the sample size is large enough that risk estimation is not too volatile.

To demonstrate the importance of selecting d , we simulate the data with $d = 3$ and set all the other parameters the same as in the first simulation. We estimate SuffPCR using $d \in \{1, 3, 5\}$ and display the results in Figure 6. When d is smaller than the true value, it is hard for SuffPCR to capture all the information contained in \mathbf{X} , thus SuffPCR has terrible prediction MSE, worse than any other methods. When d is larger than the true value, SuffPCR remains reasonable because its bias is small, but the variance will eventually increase as d increases, diminishing performance. Selecting t is not difficult in our simulations, so the results have been omitted, but it is less trivial in the real data settings.

3.2 Semi-synthetic analysis with real genomics data

The simulations in Section 3.1 explore various scenarios for the data generation process and show the performance of SuffPCR relative to the alternatives, however, they do not use any real genomic data. In this section, rather than fully generating \mathbf{X} , we create a semi-synthetic analysis wherein only the phenotypes are generated. We first performed PCA on the NSCLC data [32] and note that the first two empirical eigenvalues are relatively large, so we chose the number of PCs to be $d = 2$. We keep the top 20 rows in the empirical \mathbf{V} which have the largest norm and set the rest to 0. We then recombine and add noise. The phenotype is constructed as in the previous simulations, and the SNR is calibrated as in Section 3.1.1. Figure 7 shows the results analogous to those in Figure 4. SuffPCR continues to perform well relative to alternatives, though here, FPS has similar MSE, albeit poor feature selection.

3.3 Analysis of real genomics data

We analyze 5 microarray datasets that are publicly available and widely used as benchmarks. Four of the datasets present messenger RNA (mRNA) abundance measurements from patients with breast cancer [38, 48], diffuse large B-cell lymphoma (DLBCL) [44], and acute myeloid leukemia (AML) [8],

Method	Breast Cancer1		Breast Cancer2		DLBCL		AML		NSCLC	
	MSE	feature#	MSE	feature#	MSE	feature#	MSE	feature#	MSE	feature#
SuffPCR	0.5980	80	0.4168	121	0.7073	48	1.9568	75	0.1970	27
Lasso	0.7141	7	0.4622	39	0.6992	31	2.0998	3	0.2263	4
ElasticNet	0.6845	41	0.4517	104	0.6869	87	2.0820	5	0.2332	20
SPC	0.6188	59	0.4179	823	0.7677	67	2.3237	62	0.2795	62
ISPCA	0.8647	NA	0.5882	NA	0.9441	NA	2.3109	NA	0.2408	NA
AIMER	0.6629	76	0.4192	795	0.7003	76	1.9737	36	0.2120	50
SPCA	17.0965	212	4.7239	38	2.5980	652	31.11	1043	0.9757	387
DSPCA	0.6132	4374	0.4557	7880	0.7249	1342	1.9781	2742	0.2041	305

Table 2: Prediction MSE and number of selected features for regression of survival time on gene expression measurements

and the fifth reports microRNA (miRNA) levels from non-small cell lung cancer (NSCLC) patients [32]. The features in \mathbf{X} are gene expression measurements from microarrays.

The phenotypes Y are censored survival time in all cases, though some of the datasets also contain binary survival status indicators. Because the real valued phenotype is non-negative and right censored, we follow common practice and transform Y to $\log(Y + 1)$. Each observation is a unique patient. The first breast cancer dataset has 78 observations and 4751 genes, the second has 253 observations and 11331 genes, DLBCL has 240 observations and 7399 genes, AML has 116 observations and 6283 genes, and NSCLC has 123 observations and 939 genes.

We randomly split each dataset into 3 folds for training, validation, and testing with proportions 40%, 30% and 30% respectively. We set the number of components $d = 3$ and search over 5 log-linearly spaced λ values. Other choices for d and λ yield similar results. We train all methods on the training set, use the validation set to choose any necessary tuning parameters, and report performance of each method on the test set. We repeat the entire process (data splitting, validation, and testing) 10 times to reduce any bias induced by the random splits. In all cases, all methods were tuned to optimize validation-set MSE.

Table 2 shows the average prediction MSE and the average number of selected features for SuffPCR and any alternative methods that perform feature selection. SuffPCR works better than all the alternative methods on 4 out of 5 datasets with a comparatively small number of features selected. The DLBCL dataset tends to be difficult for both sparse and PC-based methods (as shown in the Supplement, non-sparse alternatives have much smaller prediction MSE, suggesting that many genes may play a roll in mortality rather than only a subset). SPCA is designed to maximize the variance explained by the principal components subject to a penalty on the non-sparsity, and it does not seem to work well in regression tasks. DSPCA has relatively low prediction MSE, and it does in principle perform feature selection, though it generally produces a dense model. While Ridge, Random Forests and SVM predict well in general, they do not perform any feature selection, which is a key objective here. For this reason, we report their prediction MSE in the Supplement.

To assess the potential relevance of the genes selected by SuffPCR to the cancer type from which they were identified, we further explored the DLBCL and AML datasets and extracted the selected genes. We first find the best λ via 5-fold cross-validation on all the data and then train SuffPCR with this λ . Our model selects 87 features corresponding to 32 unique genes and 2 expressed sequence tags (ESTs) for DLBCL, and 4 features corresponding to 3 unique genes and 1 EST for AML. For the genes identified from the DLBCL data, a wealth of evidence for their involvement was found in the literature.

Seventeen of the identified genes encode ribosomal proteins, overexpression of which is associated with poor prognosis [7]. A further 9 genes encoding major histocompatibility complex class II

Gene	Related ?	Reference
Ribosomal protein genes (17)	✓	Bram Ednersson et al. [7]
MHCII (9)	✓	de Charette and Houot [13]
CORO1A	✓	Li et al. [34]
FEZ1	✓	Liu et al. [35]
RAG1	✓	[37]
RYK	x	
CXCL5	x	
ESTs Hs.22635, Hs.343870	x	

Table 3: Predictive genes for DLBCL selected by SuffPCR.

Gene	Related ?	Reference
BPGM	✓	[41]
PI4KB	✓	[54]
EST Hs.321434	x	
LOC90379	✓	[19]

Table 4: Predictive genes for AML selected by SuffPCR.

(MHCII) proteins were detected, a notable finding in light of the fact that MHCII downregulation is a means by which some DLBCLs evade the immune system [13]. Discovering these large groups of similarly functioning genes illustrates the benefits of SuffPCR relative to alternatives. *CORO1A* encodes the actin-binding tumor suppressor p57/coronin-1a, the promoter of which is often hypermethylated, and therefore likely silenced, in DLBCL [34]. *FEZ1* expression has been used in a prognostic model for DLBCL [35]. *RAG1*, encoding a protein involved in generating antibody diversity, can induce specific genetic aberrations found in DLBCL [37]. *RYK* encodes a catalytically dead receptor tyrosine kinase involved in Wnt signaling and *CXCL5* encodes a chemokine. To our knowledge, neither gene has been implicated in DLBCL and thus may be of interest for further exploration. EST Hs.22635 (GenBank accession AA262469) corresponds to a portion of *ZBTB44*, which encodes an uncharacterized transcriptional repressor, while EST Hs.343870 (GenBank accession AA804270) does not appear to be contained within an annotated gene. Table 3 lists the selected genes and associated references. A listing of the genes encoding ribosomal proteins and MHCII proteins are given in the Supplement.

In the case of AML (Table 4), 3 of the 4 genes have been discussed in the literature. *BPGM*, encoding a multifunctional metabolic enzyme restricted to erythrocytes and placental cells, is upregulated in mouse models of AML [41]. *PI4KB*, encoding a lipid kinase, is amplified in breast cancer [52] and has been proposed to be a druggable AML-specific dependency [54]. *LOC90379* encodes an uncharacterized protein that is highly immunogenic in ovarian cancer serum [19]. The fourth feature discovered, Hs.321434, is an EST (GenBank accession H96229) that corresponds to an intronic sequence of an uncharacterized long noncoding RNA (lncRNA), LOC101929579, and is thus of uncertain significance. Similar listings for the discovered genes for the NSCLC and Breast Cancer 1 data are given in the Supplement without the accompanying literature review.

4 Theoretical guarantees

In the case that the data is actually generated by the sparse factor model described in [Section 3](#), SuffPCR enjoys near-optimal convergence rates. We now make the necessary assumptions concrete. We note that some of these can be weakened without meaningfully altering the main result.

- A1. $y_i = x_i^\top \beta^* + \sigma_y \epsilon_i$, $i = 1, \dots, n$, where $\epsilon_i \sim \mathcal{N}(0, 1)$, $\sigma_y > 0$.
- A2. $x_i \sim \mathcal{N}_p(0, \Sigma)$, $i = 1, \dots, n$.
- A3. $\Sigma = \mathbf{V}\mathbf{L}\mathbf{V}^\top$, is symmetric, $\mathbf{V}^\top \mathbf{V} = \mathbf{I}_p$, \mathbf{L} is diagonal.
- A4. $l_i = \lambda_i^2 I(i \leq d) + \sigma_x^2$ and $\lambda_1 - \lambda_d := \phi > 0$.
- A5. $n = \Omega((s^2 + d) \log(p))$.
- A6. $\|\text{diag}(\mathbf{V}_d \mathbf{V}_d^\top)\|_0 \leq s$ and $\min_j \{(\mathbf{V}_d \mathbf{V}_d^\top)_{jj} \vee 0\} > 2\tau$.

Theorem 1. *Suppose assumptions A1 to A6 hold and let $\hat{\beta}$ be the estimate produced by SuffPCR with $\lambda = c\lambda_1 \sqrt{\log(p)/n}$ and $t < 2\tau$. Then*

$$\frac{1}{n} \left\| \mathbf{X}(\hat{\beta} - \beta^*) \right\|_2 = \mathcal{O}_P \left(\sqrt{\frac{(s^2 + d) \log(p)}{n}} \right).$$

Theorem 2. *Suppose assumptions A1 to A6 hold and let $\hat{\beta}$ be the estimate produced by SuffPCR with $\lambda = c\lambda_1 \sqrt{\log(p)/n}$ and $2\tau > t > \tau$. Then*

$$\left| \text{supp}(\hat{\beta}) \Delta \text{supp}(\beta^*) \right| = \mathcal{O}_P \left(\frac{s^2 \log(p)}{n} \right),$$

where $A \Delta B = A/B \cup B/A$ is the symmetric difference operator and supp denotes the support set.

[Theorem 1](#) gives a convergence rate for the prediction error of SuffPCR comparable to that of Lasso though with explicit additional dependence on d . Under standard assumptions with fixed design, this dependence would not exist for Lasso. On the other hand, our results are for random design with d small, along with different constants absorbed by the big- \mathcal{O} , so a precise comparison is difficult and depends on the validity of the factor model and the covariance between features. [Theorem 2](#) shows that our procedure can correctly recover the support as long as the threshold t is chosen correctly. We note that this result is a direct consequence of Vu et al. [[50](#), [Theorem 3.2](#)]. In practice, the condition $2\tau > t > \tau$ cannot be verified, although the ‘‘elbow’’ condition we employ in the empirical examples seems to work well. Finally, we emphasize that, as is standard in the literature, these results are for asymptotically optimal tuning parameters λ , t rather than empirically chosen values. The proof of [Theorem 1](#) is given in the Supplement. These results suggest that, under this model, SuffPCR is nearly optimal as p and n grow.

5 Discussion

High-dimensional prediction methods, including regression and classification, are widely used to gain biological insights from large datasets. Three main goals in this setting are accurate prediction, feature selection, and computational tractability. We propose a new method called SuffPCR which is capable of achieving these goals simultaneously. SuffPCR is a linear predictor on estimated sparse principal components. Because of the sparsity of the projected subspace, SuffPCR usually selects a small number of features. We conduct a series of synthetic, semi-synthetic and real data analyses to demonstrate the performance of SuffPCR and compare it with existing techniques. We also prove near-optimal convergence rates of SuffPCR under sparse assumptions. SuffPCR works better than alternative methods when the true model only involves a subset of features.

References

- [1] Orly Alter, Patrick O. Brown, and David Botstein. Singular value decomposition for genome-wide expression data processing and modeling. *Proceedings of the National Academy of Sciences*, 97(18):10101–10106, 2000.
- [2] Hugues Aschard et al. Maximizing the power of principal-component analysis of correlated phenotypes in genome-wide association studies. *The American Journal of Human Genetics*, 94(5):662–676, 2014.
- [3] James Baglama and Lothar Reichel. Augmented implicitly restarted Lanczos bidiagonalization methods. *SIAM Journal on Scientific Computing*, 27(1):19–42, 2005.
- [4] Jim Baglama, Lothar Reichel, and B. W. Lewis. *irlba: Fast Truncated Singular Value Decomposition and Principal Components Analysis for Large Dense and Sparse Matrices*, 2019. R package version 2.3.3.
- [5] Eric Bair and Robert Tibshirani. Semi-supervised methods to predict patient survival from gene expression data. *PLoS Biology*, 2(4):e108, 2004.
- [6] Eric Bair, Trevor Hastie, Debashis Paul, and Robert Tibshirani. Prediction by supervised principal components. *Journal of the American Statistical Association*, 101(473):119–137, 2006.
- [7] Susanne Bram Ednersson et al. Expression of ribosomal and actin network proteins and immunochemotherapy resistance in diffuse large b cell lymphoma patients. *British Journal of Haematology*, 181(6):770–781, 2018.
- [8] L Bullinger et al. Gene expression profiling identifies new subclasses and improves outcome prediction in adult myeloid leukemia. *The New England Journal of Medicine*, 350(16):1605–1616, 2004.
- [9] Isabella Cera et al. Genes encoding SATB2-interacting proteins in adult cerebral cortex contribute to human cognitive ability. *PLoS Genetics*, 15(2):e1007890, 2019.
- [10] Sutirtha Chakraborty. Use of Partial Least Squares improves the efficacy of removing unwanted variability in differential expression analyses based on rna-seq data. *Genomics*, 111(4):893–898, 2019.
- [11] Sutirtha Chakraborty, Somnath Datta, and Susmita Datta. Surrogate variable analysis using partial least squares (SVA-PLS) in gene expression studies. *Bioinformatics*, 28(6):799–806, 01 2012.
- [12] Alexandre d’Aspremont et al. A direct formulation for sparse PCA using semidefinite programming. In *Advances in Neural Information Processing Systems*, pages 41–48, 2005.
- [13] Marie de Charette and Roch Houot. Hide or defend, the two strategies of lymphoma immune evasion: potential implications for immunotherapy. *Haematologica*, 103(8):1256–1268, Aug. 2018.
- [14] Christiaan A de Leeuw et al. Magma: Generalized gene-set analysis of GWAS data. *PLoS Computational Biology*, 11(4):e1004219, 2015.

- [15] Lei Ding and Daniel J McDonald. Predicting phenotypes from microarrays using amplified, initially marginal, eigenvector regression. *Bioinformatics*, 33(14):i350–i358, 2017.
- [16] Jonathan Eckstein and Dimitri P Bertsekas. On the Douglas-Rachford splitting method and the proximal point algorithm for maximal monotone operators. *Mathematical Programming*, 55(1-3):293–318, 1992.
- [17] Jerome Friedman, Trevor Hastie, and Robert Tibshirani. Sparse inverse covariance estimation with the graphical lasso. *Biostatistics*, 9(3):432–441, 2008.
- [18] Alex Gittens and Michael Mahoney. Revisiting the Nyström method for improved large-scale machine learning. In *Proceedings of the 30th International Conference on Machine Learning (ICML-13)*, volume 28, pages 567–575. JMLR Workshop and Conference Proceedings, 2013.
- [19] Sacha Gnjjatic et al. Seromic profiling of ovarian and pancreatic cancer. *Proceedings of the National Academy of Sciences*, 107(11):5088–5093, 2010.
- [20] Nathan Halko, Per-Gunnar Martinsson, and Joel A Tropp. Finding structure with randomness: Probabilistic algorithms for constructing approximate matrix decompositions. *SIAM review*, 53(2):217–288, 2011.
- [21] Tom Harel et al. Predicting phenotypic diversity from molecular and genetic data. *Genetics*, 213(1):297–311, 2019.
- [22] David Harville. *Matrix Algebra From a Statistician’s Perspective*. Springer, Secaucus, 1997.
- [23] Trevor Hastie, Robert Tibshirani, et al. ‘Gene shaving’ as a method for identifying distinct sets of genes with similar expression patterns. *Genome Biology*, 1(2):research0003.1–research0003.21, 2000.
- [24] Trevor Hastie, Robert Tibshirani, D. Botstein, and P. Brown. Supervised harvesting of expression trees. *Genome Biology*, 2(1):research0003–1, 2001.
- [25] Rasmus Henningsson and Magnus Fontes. SMSSVD: SubMatrix Selection Singular Value Decomposition. *Bioinformatics*, 35(3):478–486, 07 2018. doi: 10.1093/bioinformatics/bty566. URL <https://doi.org/10.1093/bioinformatics/bty566>.
- [26] Arthur E Hoerl and Robert W Kennard. Ridge regression: Biased estimation for nonorthogonal problems. *Technometrics*, 12(1):55–67, 1970.
- [27] Darren Homrighausen and Daniel J McDonald. On the Nyström and column-sampling methods for the approximate principal components analysis of large data sets. *Journal of Computational and Graphical Statistics*, 25(2):344–362, 2016.
- [28] Daniel Hsu, Sham M Kakade, and Tong Zhang. Random design analysis of ridge regression. *Foundations of Computational Mathematics*, 14(3):569–600, 2014.
- [29] Iain M Johnstone and Arthur Yu Lu. On consistency and sparsity for principal components analysis in high dimensions. *Journal of the American Statistical Association*, 104(486):682–693, 2009.
- [30] Jong Wha J. Joo et al. Efficient and accurate multiple-phenotype regression method for high dimensional data considering population structure. *Genetics*, 204(4):1379–1390, 2016.

- [31] Alamgir Kabir et al. Identifying maternal and infant factors associated with newborn size in rural Bangladesh by partial least squares (PLS) regression analysis. *PloS One*, 12(12):e0189677, 2017.
- [32] Vladimir Lazar et al. Integrated molecular portrait of non-small cell lung cancers. *BMC medical genomics*, 6(1):53, 2013.
- [33] Jeffrey T Leek and John D Storey. Capturing heterogeneity in gene expression studies by surrogate variable analysis. *PLOS Genetics*, 3(9):1–12, 09 2007.
- [34] Yinghua Li et al. Aberrant dna methylation of p57kip2 gene in the promoter region in lymphoid malignancies of b-cell phenotype. *Blood*, 100(7):2572–2577, 2002.
- [35] Ran Liu et al. Screening of key genes associated with r-chop immunochemotherapy and construction of a prognostic risk model in diffuse large b-cell lymphoma. *Molecular Medicine Reports*, 20(4):3679–3690, 2019.
- [36] Niklas Mähler et al. Gene co-expression network connectivity is an important determinant of selective constraint. *PLoS Genetics*, 13(4):e1006402, 2017.
- [37] Yi Miao, L. Jeffrey Medeiros, Yong Li, Jianyong Li, and Ken H. Young. Genetic alterations and their clinical implications in dlbc. *Nature Reviews Clinical Oncology*, 16:634–652, 2019.
- [38] Lance D Miller et al. An expression signature for p53 status in human breast cancer predicts mutation status, transcriptional effects, and patient survival. *Proceedings of the National Academy of Sciences*, 102(38):13550–13555, 2005.
- [39] Wenwen Min, Juan Liu, and Shihua Zhang. Edge-group sparse PCA for network-guided high dimensional data analysis. *Bioinformatics*, 34(20):3479–3487, 05 2018. ISSN 1367-4803. doi: 10.1093/bioinformatics/bty362. URL <https://doi.org/10.1093/bioinformatics/bty362>.
- [40] Robert Nishihara et al. A general analysis of the convergence of ADMM. In *Proceedings of the 32nd International Conference on Machine Learning*, volume 37, pages 343–352. PMLR, 2015.
- [41] Rachel L Novak et al. Gene expression profiling and candidate gene resequencing identifies pathways and mutations important for malignant transformation caused by leukemogenic fusion genes. *Experimental hematology*, 40(12):1016–1027, 2012.
- [42] Debashis Paul, Eric Bair, Trevor Hastie, and Robert Tibshirani. ‘preconditioning’ for feature selection and regression in high-dimensional problems. *The Annals of Statistics*, 36(4):1595–1618, 2008.
- [43] Juho Piironen and Aki Vehtari. Iterative supervised principal components. In *Proceedings of the Twenty-First International Conference on Artificial Intelligence and Statistics*, volume 84 of *Proceedings of Machine Learning Research*, pages 106–114. PMLR, 2018.
- [44] Andreas Rosenwald et al. The use of molecular profiling to predict survival after chemotherapy for diffuse large-B-cell lymphoma. *New England Journal of Medicine*, 346(25):1937–1947, 2002.
- [45] J Kenneth Tay, Jerome Friedman, and Robert Tibshirani. Principal component-guided sparse regression. *arXiv preprint arXiv:1810.04651*, 2018.
- [46] Robert Tibshirani. Regression shrinkage and selection via the lasso. *Journal of the Royal Statistical Society. Series B (Statistical Methodology)*, 58(1):267–288, 1996.

- [47] Michela Traglia et al. Genetic mechanisms leading to sex differences across common diseases and anthropometric traits. *Genetics*, 205(2):979–992, 2017.
- [48] Laura J Van’t Veer et al. Gene expression profiling predicts clinical outcome of breast cancer. *Nature*, 415(6871):530, 2002.
- [49] Vincent Q Vu and Jing Lei. Minimax sparse principal subspace estimation in high dimensions. *Annals of Statistics*, 41:2905–2947, 2013.
- [50] Vincent Q Vu, Juhee Cho, Jing Lei, and Karl Rohe. Fantope projection and selection: A near-optimal convex relaxation of sparse PCA. In *Advances in Neural Information Processing Systems 26*, pages 2670–2678, 2013.
- [51] Michael E Wall, Andreas Rechtsteiner, and Luis M Rocha. Singular value decomposition and principal component analysis. In *A Practical Approach to Microarray Data Analysis*, pages 91–109. Springer, 2003.
- [52] Mark G. Waugh. Amplification of chromosome 1q genes encoding the phosphoinositide signalling enzymes pi4kb, akt3, pip5k1a and pi3kc2b in breast cancer. *Journal of Cancer*, 5(9):790—796, 2014.
- [53] ChangJiang Xu et al. Multiple regression methods show great potential for rare variant association tests. *PloS One*, 7(8):e41694, 2012.
- [54] Yujia Zhou, Gregory P. Takacs, Jatinder K. Lamba, Christopher Vulpe, and Christopher R. Cogle. Functional dependency analysis identifies potential druggable targets in acute myeloid leukemia. *Cancers*, 12(12):3710, 2020.
- [55] Hui Zou. The adaptive lasso and its oracle properties. *Journal of the American Statistical Association*, 101(476):1418–1429, 2006.
- [56] Hui Zou and Trevor Hastie. Regularization and variable selection via the elastic net. *Journal of the Royal Statistical Society: Series B (Statistical Methodology)*, 67(2):301–320, 2005.
- [57] Hui Zou et al. Sparse principal component analysis. *Journal of Computational and Graphical Statistics*, 15(2):265–286, 2006.

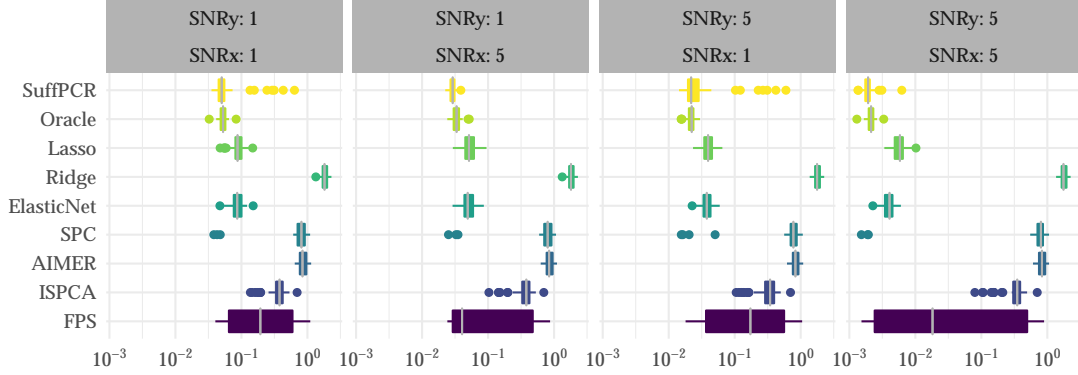


Figure 8: This figure compares the prediction MSE of SuffPCR with alternatives across different values of SNR_x and SNR_y . The x -axis is on the log scale. Boxplots are over 50 replications.

A Additional experiments and results for regression

A.1 Investigation of signal-to-noise ratio with synthetic data

In all of our synthetic examples, the data generating model has two sources of noise, one from constructing \mathbf{X} corresponding to σ_x , and the other from constructing Y , denoted σ_y . This simulation aims to control the two noise sources separately to examine their effect on the performance of SuffPCR. Note that \mathbf{X} is random unlike in standard prediction studies, so both sources of noise are important. We use SNR_x and SNR_y to denote the signal-to-noise ratio for \mathbf{X} and Y respectively. These are given by

$$\text{SNR}_x = \frac{\mathbb{E} [\|\mathbf{U}_d \mathbf{\Lambda}_d \mathbf{V}_d^\top\|_F]}{\mathbb{E} [\|\sigma_x \mathbf{E}\|_F]} = \sqrt{\frac{\text{tr}(\mathbf{\Lambda}_d^2)}{p\sigma_x^2}},$$

$$\text{SNR}_y = \frac{\mathbb{E} [\|\mathbf{X}\beta_*\|_2]}{\mathbb{E} [\|\sigma_y \epsilon\|_2]} = \sqrt{\frac{\beta_*^\top \mathbf{V}_d \mathbf{\Lambda}_d^2 \mathbf{V}_d^\top \beta_* + \sigma_x^2 \beta_*^\top \beta_*}{n\sigma_y^2}}.$$

Note that SNR_y depends not only on β_* but also on σ_x and the linear manifold through \mathbf{V}_d .

We alter the values of SNR_x and SNR_y to generate \mathbf{X} and Y while everything else is as in the first simulation. Figure 8 shows the prediction MSE for all methods on four sets of simulated data for both high and moderate combinations of SNR_x and SNR_y . When the SNR decreases, the prediction MSE of all the methods increases as expected. In all configurations, SuffPCR performs similarly to the oracle, better than Lasso or Elastic Net, while SPC is more similar to Ridge regression (though better). Interestingly, changing SNR_x and SNR_y has a similar impact on nearly all the methods except Ridge, SPC, AIMER, and ISPCA, which are nearly unaffected and uniformly worse by an order of magnitude.

A.2 Predictive genes/miRNA for additional cancers

Table 5 lists the miRNA sequences selected by SuffPCR on the NSCLC data, while Table 6 lists all the features selected by SuffPCR on the Breast Cancer1 data. Table 7 gives the prediction MSE for Ridge, Random Forests and SVM for the 5 regression datasets we examine in Section 3.3 of the manuscript. These methods predict well in general, but they do not select features.

Finally, [Table 9](#) expands on the listing in the main document, listing the genes encoding ribosomal proteins and MHCII protein which predict DLBCL survival as selected by SuffPCR.

#	Sequence	#	Sequence
1	hsa-miR-376c	21	hsa-miR-409-5p
2	hsa-miR-320c	22	hcmv-miR-US4
3	hsa-miR-299-3p	23	hsa-miR-376a
4	hsa-miR-154	24	hsa-miR-1471
5	hsa-miR-410	25	hsa-miR-411
6	hsa-miR-1182	26	bkv-miR-B1-5p
7	hsa-miR-136	27	hsa-miR-377
8	hsa-miR-379	28	hsa-miR-601
9	hsa-miR-765	29	hsa-miR-299-5p
10	hsa-miR-610	30	hsa-miR-543
11	hsa-miR-487a	31	hsa-miR-381
12	hsa-miR-136*	32	hsa-miR-329
13	hsv1-miR-H1	33	hsa-miR-760
14	hsa-miR-622	34	hsa-miR-409-3p
15	hsa-miR-659	35	hsa-miR-617
16	hsa-miR-376b	36	hsa-miR-758
17	hsa-miR-154*	37	hsa-miR-1183
18	hsa-miR-483-5p	38	hsa-miR-671-5p
19	hsa-miR-337-5p	39	hsa-miR-127-3p
20	hsa-miR-376a*		

Table 5: RNA sequences selected by SuffPCR for NSCLC data.

B Extension to classification

SuffPCR is easily extended to solve classification tasks using logistic regression (or even other classification methods). We use logistic regression as an example to show how SuffPCR performs for classification tasks. Note that the algorithm is similar to Algorithm 1 except that step 12 is replaced by the objective of logistic regression.

B.1 Synthetic data for binary classification

We first use a simulation to demonstrate the generalization of SuffPCR to solve a binary classification problem. Using the same data generating model and parameters as in the favorable scenario in Section 3.1.1 of the manuscript, we generate Y using the logistic function. As before, we choose tuning parameters with the validation set, and report the overall prediction accuracy on the test set.

[Figure 9](#) shows the classification accuracy compared to the oracle (logistic regression on the true predictors), logistic lasso, logistic ridge, and logistic FPS (logistic regression on the estimated principal components from FPS). SuffPCR has very high classification accuracy on the test set relative to the alternative methods. We also simulate classification data analogously to the other scenarios discussed in the manuscript, and the results are very similar.

#	Feature	#	Feature
1	NM_003118	15	NM_003247
2	Contig46244_RC	16	NM_004079
3	Contig55801_RC	17	NM_002775
4	M37033	18	NM_004369
5	NM_004385	19	NM_002985
6	Contig43613_RC	20	Contig43833_RC
7	Contig42919_RC	21	NM_005565
8	NM_016081	22	Contig52398_RC
9	NM_016187	23	NM_006889
10	Contig30260_RC	24	Contig66347
11	NM_000089	25	NM_000090
12	NM_000138	26	Contig25362_RC
13	NM_000393	27	NM_000560
14	Contig58512_RC	28	NM_001387

Table 6: Features selected by SuffPCR for Breast Cancer1 data.

Method	Breast Cancer1		Breast Cancer2		DLBCL		AML		NSCLC	
	MSE	feature#	MSE	feature#	MSE	feature#	MSE	feature#	MSE	feature#
Ridge	0.6331	4751	0.4330	11331	0.6766	7399	2.0451	6283	0.2105	939
Random Forest	0.5519	4751	0.3976	11331	0.6613	7399	2.0276	6283	0.2059	939
SVM linear	0.6375	4751	0.4009	11331	0.7414	7399	2.5637	6283	0.2819	939
SVM RBF	0.5602	4751	0.4448	11331	0.6684	7399	2.0106	6283	0.2080	939

Table 7: Prediction MSE for alternative methods in real genomics data analysis.

B.2 Analysis of real genomics data

We analyze 3 of the 5 real genomics datasets from Section 3.3 of the manuscript, which include a binary survival status. We use the same training test split process as in the manuscript and compare SuffPCR with logistic lasso and logistic ridge.

Method	Breast cancer1		DLBCL		AML	
	Acc.%	feature #	Acc.%	feature #	Acc.%	feature #
SuffPCR	60.95	100	60.43	103	59.39	95
Logistic Lasso	60.00	7	56.86	5	57.57	9
Logistic Ridge	58.09	4751	61.00	7399	56.97	6283

Table 8: Accuracy of survival status prediction and number of selected genes for the classification tasks on real data. Results are averaged over 10 repeated iterations.

Table 8 shows the average classification accuracy and average number of selected genes in the classification tasks. The results in the classification tasks are similar to those in regression. Again, the DLBCL dataset tends to be difficult for both sparse and PC-based methods.

GenBank AN	description
M17886	ribosomal protein, large, P1
S79522	ribosomal protein S27a
X03342	ribosomal protein L32
D23661	ribosomal protein L37
M84711	ribosomal protein S3A
L06498	ribosomal protein S20
U14973	ribosomal protein S29
M17887	ribosomal protein, large P2
L04483	ribosomal protein S21
M64716	ribosomal protein S25
L19527	ribosomal protein L27
X66699	ribosomal protein L37a
U14970	ribosomal protein S5
X64707	ribosomal protein L13
U14971	ribosomal protein S9
M60854	ribosomal protein S16
NM_022551	ribosomal protein S18
X00452	major histocompatibility complex, class II, DQ alpha 1
X00457	major histocompatibility complex, class II, DP alpha 1
X62744	major histocompatibility complex, class II, DM alpha
U15085	major histocompatibility complex, class II, DM beta
M16276	major histocompatibility complex, class II, DQ beta 1
K01171	major histocompatibility complex, class II, DR alpha
M20430	major histocompatibility complex, class II, DR beta 5
M83664	major histocompatibility complex, class II, DP beta 1
K01144	CD74 antigen (invariant polypeptide of major histocompatibility complex, class II antigen-associated)

Table 9: A listing of the genes encoding ribosomal proteins and MHCII protein which predict DLBCL survival as selected by SuffPCR.

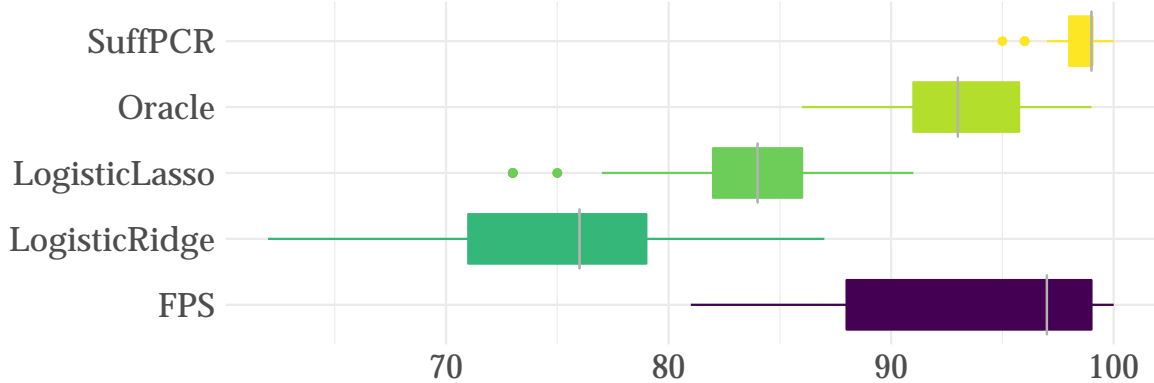


Figure 9: This figure compares the classification accuracy of SuffPCR with alternative methods. The x -axis shows the percentage of correct classifications on the test set. Boxplots are over 50 repeated simulations.

C Approximate singular value decomposition in Algorithm 1

To approximate the top j eigenvalues of a symmetric matrix \mathbf{A} , we require the k -step (partial) Lanczos bidiagonalization ($j < k$). For initial vector p_1 , this is given by

$$\mathbf{A}\mathbf{P}^{(k)} = \mathbf{Z}^{(k)}\mathbf{W}^{(k)}, \quad \mathbf{A}^\top \mathbf{Z}^{(k)} = \mathbf{P}^{(k)}\mathbf{W}^{(k),\top} + r^{(k)}e_k^\top$$

where $\mathbf{P}^{(k),\top}\mathbf{P}^{(k)} = \mathbf{Z}^{(k),\top}\mathbf{Z}^{(k)} = \mathbf{I} \in \mathbb{R}^{k \times k}$, $\mathbf{P}^{(k),\top}r^{(k)} = 0$, $\mathbf{P}^{(k)}e_1 = p_1$, and $\mathbf{W}^{(k)}$ is bidiagonal. Approximate eigenvectors and eigenvalues for \mathbf{A} can then be computed using the SVD for \mathbf{W} , which is easy because of the bidiagonal structure. However, the accuracy is closely tied to the choice of the initial vector p_1 and can be measured by the norm of the residual vector $r^{(k)}$. AIRLB [3] essentially augments the SVD of \mathbf{W} with additional information to reexpress $\mathbf{P}^{(k)}$, $\mathbf{Z}^{(k)}$ and $\mathbf{W}^{(k)}$. This process is repeated until the residual is deemed small enough.

If p_1 is in the span of the top j eigenvectors of \mathbf{A} , then no iteration will be necessary, and the approximation is exact. So, within our ADMM, when the span of the eigenvectors for $\mathbf{B} - \mathbf{C} + \mathbf{S}/\rho$ is similar across iterations, previous iterates can be used as initializations for the restarted Lanczos procedure. Thus, as we loop through the ADMM steps, these initializations improve the speed subsequent decompositions.

This modification significantly improves the per-iteration efficiency of the algorithm while still converging in a few dozen iterations. Note that ADMM will still converge (though in perhaps more iterations) if some or all of the steps are implemented approximately [16]. In particular, by approximating the projection of \mathbf{Q} , $\text{Proj}_{\mathcal{F}^d}(\mathbf{Q})$, with $\widetilde{\text{Proj}}_{\mathcal{F}^d}(\mathbf{Q})$, ADMM will converge provided

$$\sum_{k=1}^{\infty} \left\| \text{Proj}_{\mathcal{F}^d}(\mathbf{Q}^{(k)}) - \widetilde{\text{Proj}}_{\mathcal{F}^d}(\mathbf{Q}^{(k)}) \right\| < \infty.$$

Nishihara et al. [40] suggests linear convergence for ADMM, and our experience is that this case remains linear despite the approximation.

D Proofs

To prove Theorem 1, we first need the following technical lemma.

Lemma 1. *Let $\Xi = \mathbf{Z}\mathbf{Z}^\top$ be the orthogonal projector on to the d -dimensional subspace of \mathbb{R}^p spanned by \mathbf{Z} with $\mathbf{Z}^\top\mathbf{Z} = \mathbf{I}_d$. Let $b \in \mathbb{R}^n$ and $\mathbf{A} \in \mathbb{R}^{n \times p}$. Then, defining $\hat{x} := \operatorname{argmin}_x \|\mathbf{A}\mathbf{Z}x - b\|_2^2$,*

$$\begin{aligned} \mathbf{Z}\hat{x} &= \mathbf{Z}(\mathbf{A}\mathbf{Z})^+b = (\mathbf{A}\Xi)^+b \\ &= \operatorname{argmin}_y \|\mathbf{A}\Xi y - b\|_2^2 =: \hat{y}, \end{aligned}$$

where \mathbf{Q}^+ is the Moore-Penrose generalized inverse of \mathbf{Q} .

Proof of Lemma 1. We have

$$\begin{aligned} \hat{y} &:= (\mathbf{A}\Xi)^+b = \Xi(\mathbf{A}\Xi)^+b = \mathbf{Z}\mathbf{Z}^\top(\mathbf{A}\mathbf{Z}\mathbf{Z}^\top)^+b \\ &= \mathbf{Z}\mathbf{Z}^\top\mathbf{Z}(\mathbf{A}\mathbf{Z})^+b = \mathbf{Z}(\mathbf{A}\mathbf{Z})^+b =: \mathbf{Z}\hat{x}. \end{aligned}$$

Here, the first equality is a standard property of idempotent matrices and the third follows from [22, Thm. 20.5.6]. \square

Proof of Theorem 1. Write $\mathbf{\Pi} = \mathbf{V}_d\mathbf{V}_d^\top$ and $\hat{\mathbf{\Pi}} = \hat{\mathbf{V}}_d\hat{\mathbf{V}}_d^\top$ for the orthogonal projectors onto the column span of the population quantity \mathbf{V}_d and the estimate produced by Algorithm 2 respectively. Let

$$\tilde{\gamma} = \operatorname{argmin}_\gamma \|\mathbf{X}\mathbf{V}_d\gamma - Y\|_2^2,$$

and define $\tilde{\beta} = \mathbf{V}_d\tilde{\gamma}$. Note that $\beta_* \in \operatorname{col}(\mathbf{V}_d)$ and $\hat{\beta} \in \operatorname{col}(\hat{\mathbf{V}}_d)$ as $\beta_* = \mathbf{V}_d\mathbf{L}_d^{-1}\mathbf{\Lambda}_d\Theta =: \mathbf{V}_d r$ and $\hat{\beta} = \hat{\mathbf{V}}_d\hat{\gamma}$. Then,

$$\begin{aligned} &\|\mathbf{X}(\beta_* - \hat{\beta})\|_2^2 \\ &= \|\mathbf{X}(\beta_* - \tilde{\beta})\|_2^2 + \|\mathbf{X}(\tilde{\beta} - \hat{\beta})\|_2^2 \\ &= \|\mathbf{X}(\mathbf{V}_d\gamma_* - \mathbf{V}_d\tilde{\gamma})\|_2^2 + \|\mathbf{X}(\mathbf{V}_d\tilde{\gamma} - \hat{\mathbf{V}}_d\hat{\gamma}_d)\|_2^2 \\ &= \|\mathbf{X}\mathbf{V}_d(\gamma_* - \tilde{\gamma})\|_2^2 + \|\mathbf{X}(\mathbf{\Pi}\tilde{\beta} - \hat{\mathbf{\Pi}}\hat{\beta})\|_2^2, \end{aligned}$$

where the last line follows by Lemma 1.

Now, $\mathbf{X}\hat{\beta} = \hat{Y} \in \operatorname{col}(\mathbf{X}\hat{\mathbf{\Pi}})$ and $\mathbf{X}\tilde{\beta} = \tilde{Y} \in \operatorname{col}(\mathbf{X}\mathbf{\Pi})$, and $\operatorname{col}(\mathbf{X}\mathbf{\Pi}) \subset \operatorname{col}(\mathbf{X}) \cap \operatorname{row}(\mathbf{\Pi}) = \operatorname{col}(\mathbf{X}) \cap \operatorname{col}(\mathbf{\Pi})$ (because $\mathbf{\Pi}$ is symmetric). Thus, we have that $\hat{Y} \in \operatorname{col}(\mathbf{X}\hat{\mathbf{\Pi}}) \subset \operatorname{col}(\mathbf{X}) \cap \operatorname{col}(\hat{\mathbf{\Pi}})$ and $\tilde{Y} \in \operatorname{col}(\mathbf{X}\mathbf{\Pi}) \subset \operatorname{col}(\mathbf{X}) \cap \operatorname{col}(\mathbf{\Pi})$. By linearity, there exist orthogonal projectors \mathbf{Q} and \mathbf{R} such that $\hat{Y} = \mathbf{Q}Y$ and $\tilde{Y} = \mathbf{R}Y$. Therefore,

$$\begin{aligned} \|\mathbf{X}(\mathbf{\Pi}\tilde{\beta} - \hat{\mathbf{\Pi}}\hat{\beta})\|_2^2 &= \|\hat{Y} - \tilde{Y}\|_2^2 \\ &= \|(\mathbf{Q} - \mathbf{R})Y\|_2^2 \\ &\leq \|\mathbf{Q} - \mathbf{R}\|_F^2 \|Y\|_2^2 \\ &\leq \|\mathbf{\Pi} - \hat{\mathbf{\Pi}}\|_F^2 \|Y\|_2^2, \end{aligned}$$

where the first inequality is Hölder's inequality for the Frobenius norm. For the second, since \mathbf{Q} and \mathbf{R} are (orthogonal) projectors onto subspaces of $\text{col}(\mathbf{\Pi})$ and $\text{col}(\widehat{\mathbf{\Pi}})$, it must be that $\|\mathbf{Q} - \mathbf{R}\|_F \leq \|\mathbf{\Pi} - \widehat{\mathbf{\Pi}}\|_F$.

Now, since $\widehat{\mathbf{\Pi}}$ is a solution to the Fantope projection problem under Assumptions A1–A6, we can invoke [50, Cor. 3.3] to get that

$$\|\mathbf{\Pi} - \widehat{\mathbf{\Pi}}\|_F = \mathcal{O}_P\left(s\sqrt{\log(p)/n}\right)$$

while $\|Y\|^2/n = \mathcal{O}_P(1)$.

Turning now to $\|\mathbf{X}\mathbf{V}_d(\gamma_* - \tilde{\gamma})\|_2^2$, $\tilde{\gamma}$ is simply the ordinary least squares regression estimate under random design. Thus by, for example, [28, Theorem 1 and subsequent remarks],

$$\|\mathbf{X}\mathbf{V}_d(\gamma_* - \tilde{\gamma})\|_2^2 = \mathcal{O}_P(\sigma^2 d/n).$$

Combining these terms gives the result. □